Simulation models of dengue transmission in Funchal, Madeira Island: influence of seasonality

Donald Salami[1*], César Capinha[2], Carla Alexandra Sousa[1*], Maria do Rosário Oliveira Martins[1], Cynthia Lord[3*]

[1] Global Health and Tropical Medicine, Instituto de Higiene e Medicina Tropical, Universidade Nova de Lisboa, Lisbon, Portugal

[2] Centro de Estudos Geográficos, Instituto de Geografia e Ordenamento do Território, Universidade de Lisboa, Lisbon, Portugal

[3] Florida Medical Entomology Laboratory, Institute of Food and Agricultural Sciences, University of Florida, Vero Beach, Florida, United States.

* Corresponding author

Email: donald.salami@gmail.com (DS)

casousa@ihmt.unl.pt (CS), clord@ufl.edu (CL)

Abstract

The recent emergence and established presence of *Aedes aegypti* in the Autonomous Region of Madeira, Portugal, was responsible for the first autochthonous outbreak of dengue in Europe. The island has not reported any dengue cases since the outbreak in 2012. However, there is a high risk that an introduction of the virus would result in another autochthonous outbreak given the presence of the vector and permissive environmental conditions. Understanding the dynamics of a potential epidemic is critical for targeted local control strategies.

Here, we adopt a deterministic model for the transmission of dengue in *Aedes aegypti* mosquitoes. The model integrates empirical and mechanistic parameters for virus transmission, under seasonally varying temperatures for Funchal, Madeira Island. We examine the epidemic dynamics as triggered by the arrival date of an infectious individual; the influence of seasonal temperature mean and variation on the epidemic dynamics; and performed a sensitivity analysis on the following quantities of interest: the epidemic peak size, time to peak and the final epidemic size.

Our results demonstrate the potential for summer to early winter transmission of dengue, with the arrival date significantly affecting the distribution of the timing and peak size of the epidemic. Mid-summer to early autumn arrivals are more likely to produce larger epidemics within a short peak time. Epidemics within this favorable period had an average of 18% of the susceptible population infected at the peak, at an average peak time of 70 days. We also demonstrated that seasonal temperature variation dramatically affects the epidemic dynamics,

with warmer starting temperatures producing peaks more quickly after an introduction and larger epidemics. Overall, our quantities of interest were most sensitive to variance in the date of arrival, seasonal temperature, biting rate, transmission rates, and the mosquito population; the magnitude of sensitivity differs across quantities.

Our model could serve as a useful guide in the development of effective local control and mitigation strategies for dengue fever in Madeira Island.

Author Summary

The presence of *Aedes aegypti* mosquitoes in Madeira Island had recently caused the first local outbreak of dengue in Europe. The island is at risk of another local transmission if triggered by the introduction of the dengue virus by an infected person. Using a mathematical model for the transmission of dengue, we examine the dynamics of a potential epidemic triggered by the arrival of an infected person on the island. We also examine the impact of seasonal temperature variation on the epidemic dynamics. Our results show the potential for summer to early winter transmission of dengue on the island, and that the arrival date of an infectious person affects the distribution of the timing and peak size of the epidemic. Arrival dates during mid-summer to early autumn were more likely to produce larger epidemic peak size within a short time. We also show that seasonal temperature variation dramatically affects the epidemic dynamics. With warmer starting temperatures, epidemics peak more rapidly and produce a larger epidemic size. Our model could be useful to estimate the risk of an epidemic outbreak and as a guide for local control and mitigation strategies for dengue on the island.

Introduction

Dengue is notably the most important mosquito-borne viral disease, with approximately half the world's population at risk of infection [1]. This arboviral disease, caused by a virus of the Flaviviridae family, has gained renewed global attention due to its wide geographical spread and increased burden in recent years. The spread of the disease is in concordance with the geographical expansion of its primary vector (i.e. *Aedes aegypti*), characterized by the presence of a suitable climate and increase in global trade and travel [2, 3].

A paradigmatic example of the recent spread of dengue and its epidemic potential was demonstrated in Madeira Island, an autonomous region of Portugal (S1 Fig), with an estimated population size of 270,000. *Aedes aegypti* was first detected in Funchal, the capital city of Madeira Island, in 2005 and by October 2012 the island reported its first autochthonous case of Dengue serotype 1 (DENV 1) [4]. The importance of this epidemic is demonstrated by three main reasons: (1) It was the first sustained autochthonous transmission of dengue in the European Union since the 1920s [5]; (2) its size, with 1080 confirmed cases (of the 2168 probable cases reported) and 78 cases reported in 13 other European countries in travelers returning from Madeira [6]; and (3) the rapid time course of the epidemic, the epidemic peaked within a month after the official report of the first case in October [7] with a rapid decline thereafter and was extinct by March 2013.

To understand the complexities of this outbreak, Lourenco and Recker [8] developed an ento-epidemiological mathematical model to explore the ecological conditions and transmission dynamics. Their findings suggest the virus was introduced over a month before cases were

reported (in August). In their model, asymptomatic circulation occurred before the two initial autochthonous cases were reported in October, maintaining the virus in the population. Furthermore, their findings indicate that the transmission dynamics and eventual epidemic burnout was driven predominantly by the influence of temperature on the life-history traits of the mosquitoes (incubation period, mosquito mortality and aquatic developmental rates). The seasonal drop in autumn temperatures led to a reduction of the vectorial capacity and effectively stopped the virus propagation.

Their findings are consistent with previous experimental work addressing the strong influence of temperature on the life-history traits of the mosquitoes and arbovirus transmissions [9-12]. Likewise, many existing mechanistic transmission models have integrated the effects of temperature on mosquito traits to understand how it influences the probability and magnitude of dengue transmissions [13-17]. Other recent work examined the influence of seasonal variation in temperature on the epidemic magnitude and duration [18, 19]. These models emphasize the strong, nonlinear (often unimodal) influence of temperature and seasonality on dengue transmission and epidemic dynamics.

Expanding on previous work, we here explore the impact of seasonal temperature variations on the potential epidemic dynamics on Madeira Island. It is imperative to explore the influence of seasonality, as Madeira Island presents with a range of contrasting bioclimates as a result of its heterogeneous landscape and strong influence from the Gulf Stream and Canary current [20]. The southern coastal regions of the island (including Funchal), at low altitudes, have higher annual temperatures in comparison to the northern coastal regions or inland regions

with higher altitudes and lower annual temperatures [20, 21]. Although the island has not reported any dengue cases since the outbreak in 2012, new introductions would likely result in local transmission given the presence of the vector and permissive environmental conditions. A recent vector competence study with *Aedes aegypti* from Madeira reported virus transmission potential (virus in saliva) from 2 Madeira populations, although the proportions transmitting was low (transmission rate of 18%, 14 days post-infection) [22]. This demonstrates the potential risk for a local transmission of from a different serotype dengue, if introduced on the island. With an increase in co-circulation of all dengue serotypes (DENV 1-4) worldwide [23, 24], and Madeira's increasing lure as a popular year-round travel destination, a potential introduction is likely [25].

We incorporate a standard deterministic SEI-SEIR transmission model parameterized from existing literature and available field data. The main goals of this model are: (1) to examine the epidemic dynamics in Funchal, Madeira as triggered by the arrival of an infectious individual at different time points during the year; and (2) to examine the influence of seasonal temperature mean and variation on epidemic dynamics. To do this, we employed a different modeling framework from that of [8], in that our model explicitly accounts for seasonality and temperature dependence in the transmission dynamics. Likewise, we explore epidemiologically relevant outcomes of epidemic size, peak incidence and time to peak, rather than basic reproduction number or vectorial capacity, which are more complex measures of epidemic dynamics.

Methods

Model framework

We adopt a deterministic compartmental vector-host transmission model exploring chikungunya virus invasion in Florida, United States with *Aedes aegypti* and *Aedes albopictus* mosquitoes, from Lord et al. (unpublished work). This was adapted into a standard SEI-SEIR transmission model with one vector, similar to others used in modeling dengue transmission (e.g. in [26-29]).

The SEI component of our model describes the vector population, represented as susceptible (S_v), exposed (E_v), and infectious (I_v). Our models explicitly consider a single vector and a single life stage, i.e. adult females of *Aedes aegypti*. Mosquitoes enter the susceptible class through a recruitment term, based on observed seasonality patterns from field data in Funchal [30]. The recruitment term does not explicitly model the aquatic (eggs, larvae, and pupae) stage of mosquitoes and is not linked to the current population size, but explicitly includes seasonality in recruitment to the adult female population. A susceptible mosquito moves into the exposed class (E_v), after biting an infectious human and becoming infected with dengue virus. After a temperature-dependent extrinsic incubation period, surviving mosquitoes get transferred to the infectious class (I_v). They remain in the infectious class until death, due to the assumption of the absence of immune response. Mosquitoes leave the system through a temperature-dependent mortality function. We assume the virus infection does not affect the lifespan of the mosquitoes and that there is no significant vertical transmission.

The SEIR component of our model describes the human population represented as susceptible (S_h), exposed (infected but not infectious) (E_h), infectious (I_h), and recovered (immune) (R_h). Our model assumes the human population (N_h) to be constant, not subject to demography as we considered a single outbreak with a duration in the order of a year. A susceptible individual enters the exposed class (E_h) after being successfully infected, by an infectious mosquito bite. We do not explicitly account for repeated biting, interrupted feeds or alternative host preferences. We also assume that not every infectious bite leads to successful human infection. Once a human individual is exposed, they enter an intrinsic incubation period, until they become infectious. They then move to the infectious class (I_h) and can transmit the virus back to a susceptible mosquito. We assumed a single infectious class and did not further discriminate between the symptomatic or asymptomatic individuals as previous evidence demonstrates that asymptomatic individuals can transmit the virus [31]. We assume that humans stay infectious for a period after which they recover. Once a human individual enters the recovered/immune class (R_h), we assume a lifelong immunity, as multiple co-circulating serotypes of dengue virus was not considered. A resulting schematic representation of the model is shown in Fig 1.

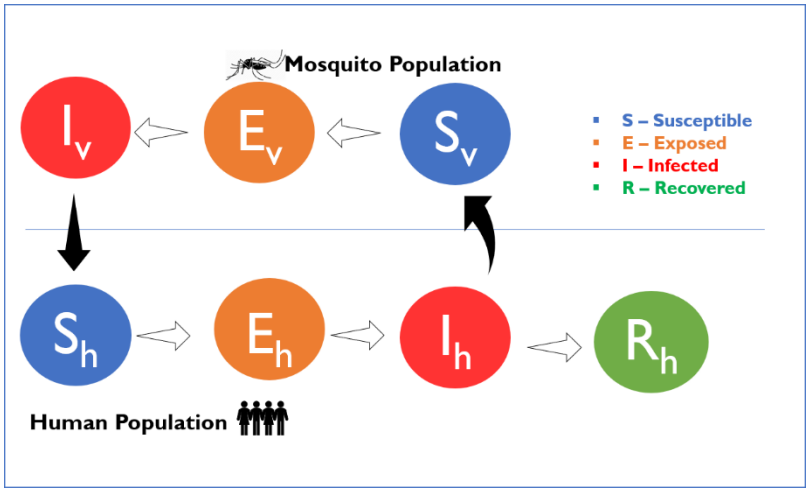

Fig 1. Schematic representation of the model. S_v, E_v, and I_v represent the susceptible, exposed, and infectious compartments of the mosquito population. S_h, E_h, I_h, and R_h represent the susceptible, exposed, infectious, and recovered compartments of the human population, respectively. The outline arrows are the transition from one compartment to the next, and the black filled arrows are the direction of transmission.

Model equations

Our model is defined by the following ordinary differential equations:

$$\frac{dS_v}{dt} = \rho - \frac{a(t)\,\beta_{h\to v}}{N_h} I_h S_v - \mu_v S_v \qquad (1)$$

$$\frac{dE_v}{dt} = \frac{a(t)\,\beta_{h\to v}}{N_h} I_h S_v - \gamma_v E_v - \mu_v E_v \qquad (2)$$

$$\frac{dI_v}{dt} = \gamma_v E_v - \mu_v I_v \qquad (3)$$

$$N_v = S_v + E_v + I_v \qquad (4)$$

$$\frac{dS_h}{dt} = -\frac{a(t)\,\beta_{v\to h}}{N_h} S_h I_v \qquad (5)$$

$$\frac{dE_h}{dt} = \frac{a(t)\,\beta_{v\to h}}{N_h} S_h I_v - \gamma_h E_h \qquad (6)$$

$$\frac{dI_h}{dt} = \gamma_h E_h - \eta_h I_h \qquad (7)$$

$$\frac{dR_h}{dt} = \eta_h I_h \qquad (8)$$

$$N_h = S_h + E_h + I_h + R_h \qquad (9)$$

Here, the coefficient ρ is the mosquito recruitment term (expanded below); $a(t)$ is the biting rate per unit time; $\beta_{h\to v}$ and $\beta_{v\to h}$ are the human-to-mosquito and mosquito-to-human transmission rates, respectively; $1/\gamma_h$ and $1/\eta_h$ represent the intrinsic incubation and human infectivity periods; $1/\gamma_v$ and μ_v represent the extrinsic incubation period and mortality rate for mosquitoes (temperature-dependent, details below). The state variables and parameters used for our model are displayed in Tables 1 and 2, respectively.

Table 1. State variables for the model.

Variables	Description
S_v	Number of susceptible mosquitoes
E_v	Number of exposed mosquitoes
I_v	Number of infectious mosquitoes
N_v	Total mosquito population size
S_h	Number of susceptible humans
E_h	Number of exposed humans
I_h	Number of infectious humans
R_h	Number of recovered humans
N_h	Total human population size

Table 2. Definitions and ranges of the model's parameters.

Parameter	Description	Default Value	Range	Reference
$\boldsymbol{r_\delta}$	Number of mosquitoes per host in the unimodal peak phase	2	2 – 6	[8, 32, 33]
$\boldsymbol{p_{base}}$	Proportion of mosquitoes in baseline recruitment	0.05		[8, 34]
$\boldsymbol{iv}$	The interval between baseline pulses (days)[1]	5	2 – 7	[34]
$\boldsymbol{q}$	Timing of unimodal peak (days)[1]	220	209 –230	[34]
$\boldsymbol{\sigma}$	The variance of the unimodal peak (days)[1]	29		[34]

$\boldsymbol{R_{tot}}$	Total mosquito recruitment (population size)[2]			Calculated based on default value and range for r_δ above. Used in the sensitivity analysis.
$\boldsymbol{a}$	Mosquito biting rate	0.4	0.33 – 1.0	[35, 36]
$\boldsymbol{\beta_{h\to v}}$	Rate of transmission from human to mosquito	0.33	0.1 – 0.75	[27, 32, 37]
$\boldsymbol{\beta_{v\to h}}$	Rate of transmission from mosquito to human	0.33	0.1 – 0.75	[27, 32, 37]
$\boldsymbol{\mu_v}$	Mortality rate of mosquitoes under optimal temperatures [3]	0.04	0.02 – 0.06	[13, 17]
$\boldsymbol{\mu_{vs}}$	The slope of mortality function	0.05		[13, 38]
$\boldsymbol{\gamma_v}$	Virus extrinsic incubation rate (at 22.5°C)	0.04	0.04 – 0.07	[17, 39]
$\boldsymbol{\gamma_{vs}}$	Slope of extrinsic incubation function	0.008		[39]
$\boldsymbol{1/\gamma_h}$	Intrinsic incubation period (days)	6		[40, 41]
$\boldsymbol{1/\eta_h}$	Human infectious period (days)	4		[8, 36, 42, 43]
$\boldsymbol{N_h}$	The population size of humans (constant)	30000		[44]
$\boldsymbol{t_{crit}}$	Date of arrival of infectious human (days)[4]	181	1 – 365	
$\boldsymbol{T_{mean}}$	Mean annual temperature (°C)	20	15 - 30	[45, 46]
$\boldsymbol{T_{range}}$	Temperature range (°C)[5]	5	0 - 15	[45, 46]

[1] Default value and range are estimates to reflect the observed seasonal activity, not an explicit fit to the island's entomological data; [2] See equation 15, also note this parameter was used in the sensitivity analysis to allow

estimation of the relative importance of the total recruitment; [3] Mosquitoes optimal survival range: ($15 > T < 30$°C); [4] Where t_{crit} = 1, calendar date is February 15; hence t_{crit} of 181 is August 15; while 365 is February 14 (i.e. a complete annual period). [5] Temperature range is given by($T_{max} - T_{min}$).

Mosquito recruitment. The coefficient (ρ) in equation (1) above is the daily recruitment term of susceptible mosquitoes. The total number of female mosquitoes recruited into the population over the year is divided into two main phases: baseline, year-round recruitment, and a unimodal peak season recruitment. This is based on the seasonal pattern of mosquitoes on the island observed from the *Aedes aegypti* mosquito entomological surveillance by the Institute of health administration, IP-RAM and the Funchal natural history museum [30, 47]. Weekly mosquito trap data is geo-processed and spatial analyzed to identify areas with mosquito activity based on the presence/absence of eggs, the number of eggs and adult mosquitoes captured [30].

Visual inspection of the entomological data for the years 2012 – 2019 (weekly time-series graphs of the cumulative number of eggs and adult mosquitoes, see S2 - S5 Figs) [34] demonstrate a unimodal seasonal pattern for mosquito activity during the entomological season. The unimodal peak starts around June through to early December, with other months of the year (i.e. January to May) having little to no activity. Using a Gaussian curve, we estimated the timeline for our unimodal peak recruitment to reflect this seasonal pattern as best possible.

Actual quantifications of mosquito population density remain a grey area. However, the majority of dengue models [8, 27, 32, 33, 48] have adopted the use of a mosquito-to-human ratio

of 2:1. We adopted this framework for setting the estimated number of mosquitoes recruited during the unimodal peak season (r_δ). From the derived number of mosquitoes recruited during the peak season, we assumed an additional 5% to be added in the baseline, year-round recruitment (p_{base}). The recruitment of susceptible mosquitoes is specified by the following equations:

$$\rho(t) = \rho_b\ (t) + R_{peak}\delta(t) \qquad (10)$$

Where,

$$\delta\,(t) = \frac{1}{2\pi\sigma_k}\ exp\left(\frac{1(q_k - t)^2}{2\sigma_k^2}\right) \qquad (11)$$

$$\rho_b(t) = \frac{R_{base}}{iv} \qquad (12)$$

$$R_{peak} = r_\delta N_h \qquad (13)$$

$$R_{base} = R_{peak} p_{base} \qquad (14)$$

$$R_{tot} = R_{peak} + R_{base} \qquad (15)$$

Here, $\rho(t)$ represents the number of adult female mosquitoes recruited per time step; $\delta\,(t)$ is a Gaussian distribution for the number of mosquitoes added to the population daily, during the unimodal peak season; $\rho_b(t)$ is the number of mosquitoes added to the population at intervals (iv) during the all-year-round recruitment. R_{peak} is the total number of mosquitoes recruited during the unimodal peak season; R_{base} is the total number of mosquitoes recruited

during the baseline, year-round recruitment; R_{tot} is the total number of mosquitoes recruited into the population over the year.

Seasonal forcing. To introduce seasonality in our model, we allowed temperature to vary over time by sinusoidally forcing [49]. The daily mean temperature was modeled as a cosine curve with a period of 365 days as specified below:

$$T\ (t) = \frac{T_{max} - T_{min}}{2} * \left(-\cos\left(\frac{2\pi(t-\omega)}{365}\right)\right) + T_{mean} \qquad (16)$$

Here, T_{max}, T_{mean}, and T_{max} are the average daily maximum, mean, and minimum temperatures over the year, (t) is time measured in days and (ω) is the phase shift to align the cosine function with the seasonal factors in Funchal. For our temperature model calibration, we extracted a 10 year (2008 – 2018) historical daily from Weather Underground [45]. We then calculated the 10-year historical average of the mean, minimum, and maximum for each day of the year (excluding February 29), before estimating temperature seasonality. This provided a range of the average daily temperature over a calendar year for the period. Utilizing the mean, minimum, and maximum annual average temperature, we set estimates for our seasonality parameters. To fit the sinusoidal model, we considered the occurrence of the coldest and hottest day across the years, to determine a good starting point. The occurrence of the coldest day had fewer fluctuations mostly occurring on February 15; hence we set our start point and phase shift to this day, reflecting the long-term average conditions in Funchal, Madeira (T_{max}= 22° C,

T_{mean}= 20°C, T_{min}= 17°C). S6 Fig shows a fit of the sinusoidal curve to the historical temperature seasonality.

Temperature-dependent parameters. The extrinsic incubation period (γ_v) is modeled to be temperature-dependent, modified from [50]. Using a linear temperature function, specified by a slope (γ_{vs}), the rate near the midpoint of the plausible temperatures range for vectorial capacity (set at 22.5°C), and a defined lower temperature threshold (set at 10ºC, at which point (γ_v) equals zero). Mortality rates (μ_v) for mosquitoes was modeled as a function of temperature using a mechanistic thermal response curve as described in [13]. They fitted their data as a complex polynomial resulting in a basin-shaped curve, with optimal temperature for mosquito's survival set at a range of $15℃ > T < 30℃$. Based on preliminary exploration of changes to the mortality function, we modified the fitted polynomial to a piecewise linear curve with fixed, minimal mortality in the same temperature range. Mortality rate then increases quickly and linearly at temperatures outside this lower and upper bound, as specified by the function slope (μ_{vs}).

Quantities of interest (QOI)

We simulated the model under default starting conditions (see S1 Appendix) and given that a simulation evolves into an epidemic (defined as ($I_h > 2$), after the virus introduction), we analyze for the following quantities of interest (QOI): the epidemic peak size (maximum human infected ($maxI_h$) at any given point during the simulation); time to peak infection in humans (time from introduction to $maxI_h$, as $tmaxI_h$); the final epidemic size, which represents a

measure of epidemic suitability (cumulative proportion of humans infected, $cumI_h/N_h$, at the final time step).

Initial introduction and epidemic dynamics

Firstly, we examine the variability in epidemic dynamics, as a result of different arrival dates of an infectious human in a susceptible population. To do this, we ran simulations for all 365 calendar days of the year, with all other parameters fixed at their default values (Table 2) and default starting conditions (S1 Appendix). Each simulation was started on February 15 (the phase shift in the annual cycle) and ran for 2 years.

Seasonal variance and epidemic dynamics

Next, we examine the epidemic dynamics as a function of seasonal temperature variation. Utilizing the same compartmental framework with default starting conditions and parameter values, we ran sets of simulations under two different temperature regimes [18]. First, we simulated a set of temperature regimes as observed in the historical decadal data for Funchal, Madeira. The mean temperature varied from 19.0 ºC to 21.0 ºC in increments of 0.2 ºC, while the temperature range (i.e. $T_{max} - T_{min}$) varied from 4.0 ºC to 6.0 ºC, in the same increments of 0.2 ºC, resulting in 121 simulation runs. The variability in epidemic dynamics is then examined as a function of starting temperature. Starting temperature is defined as the temperature on the day of introduction of the virus (t_{crit}), as derived from the temperature curves.

Next, we simulate a wider set of temperature regimes to examine plausible future forcing scenarios based on near-term projections of seasonal temperature changes in the region of Madeira Island. Near term projection refers to projected annual mean temperature changes for the period 2016–2035 relative to a reference period 1986–2005 [46, 51]. Mean temperature was varied between 15.0 ºC to 30.0 ºC in increments of 0.2 ºC, while range varied from 0.0 ºC to 15.0 ºC in increments of 0.2 ºC (i.e. a total of 5776 simulation runs). It is worth noting that most of the temperatures in this regime are outside projected changes for the island's region, and very unlikely to occur in Funchal. However, by simulating a wider set of temperature regimes, we can characterize uncertainties and probable outcomes of a local epidemic across other regions on the island. This also allows us to simulate similar extreme temperature conditions already recorded on the Funchal in recent times (for example, high temperatures of 37.8ºC on August 5, 2016, and 26.5 ºC on December 5, 2018 [52, 53]).

Model sensitivity analysis

To characterize the model parameters exerting the most influence on our quantities of interest, we performed a variance-based global sensitivity analysis, using a combination of Latin hypercube sampling (LHS) and a multi-model inference on regression-based models (See S2 Appendix for details). The sensitivity analysis considered the main effects and pairwise (first-order) interactions of input parameters on our quantities of interest. LHS sampling was programmed in MATLAB [54], while the multi-model inference analysis was done using the *glmulti* R package [55, 56].

Results

Initial introduction and epidemic dynamics

We examined the timing and size of the epidemic peak as a function of different arrival dates of an infectious human into the susceptible population. An epidemic outbreak occurred only for simulated arrival dates in July to mid-December; with the first epidemic occurring on July 1. Most simulations responded unimodally with peaks occurring a few weeks after the arrival of an infectious human, this was typical for summer and autumn arrivals (Figs 2A and 2B). However, some simulations responded bimodally, i.e. an initial small outbreak, then a prolonged low-level transmission until another outbreak occurs (Figs 2C and 2D). This prolonged transmission was typical for arrival dates at the end of autumn and beginning of the winter seasons (i.e. arrival dates in November and early December).

We examine this behavior further by comparing the disease progression in the human population with that of the mosquito population (Fig 2D). Simulations with an arrival date of the infectious human in November/December had a lower chance to evolve into a unimodal outbreak, because of the depletion of the mosquito population. Following the initial outbreak, a low transmission is maintained until the next seasonal peak recruitment of the mosquitoes, before another outbreak. Suggesting that the virus can remain viable within the population at low rates, until the next favorable season for transmission. This also means the dynamics of the epidemic, is also modulated by the temporal dynamics of the mosquito population, however, this is not the focus of our analysis.

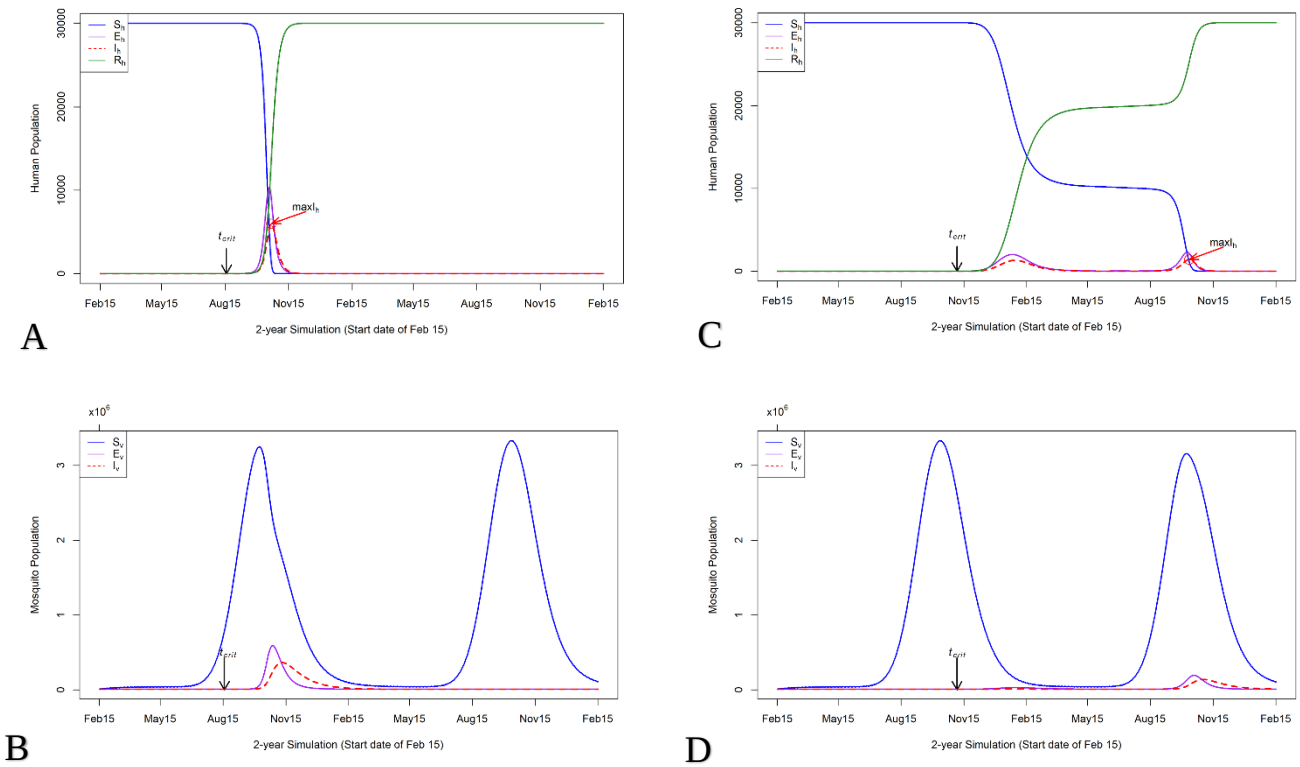

Fig 2. The epidemic progression in the human and mosquito populations. The y-axis is the number of humans or mosquitoes in the simulation and the x-axis is the 2-year simulation dates with start date of February 15. t_{crit} = arrival date of infectious human; $maxI_h$ = the epidemic peak size, the maximum human infected at any given point during the simulation. (A) indicates the disease progression in the human population, for an arrival date of an infectious human on August 17. (C) indicates disease progression for an arrival date of an infectious human on November 5. (B) and (D) show the disease progression in the mosquito population for the respective dates of arrival. (A) shows a classical rapid epidemic, with a unimodal response, with the peak occurring few weeks after virus introduction; while (C) shows a prolonged period of lower-level transmission, resulting in a bimodal response. Default parameters from Table 2 were used for these simulations, except for dates of arrival of infectious human.

Fig 3 shows our QOI, for all simulation dates resulting in an epidemic. Epidemic peak size monotonically decreases as a function of the date of arrival until early November (end of the autumn season) and reverses to an increase. In contrast, epidemic peak time demonstrates a J-

shaped curve, with the increase starting at the end of September (beginning of Autumn), with a steep spike in early November. In part, these discontinuities are reflections of scoring each run for a single peak; and corresponds to the model behavior shifts from the classical rapid unimodal epidemic, to the bimodal and prolonged epidemic. Overall, arrival dates in the summer season produced higher peak incidence with short epidemic peak timing.

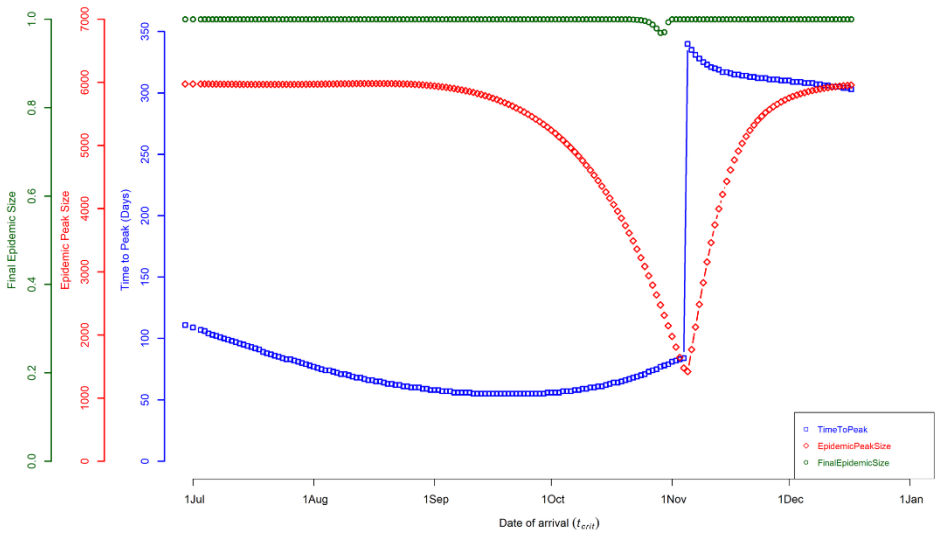

Fig 3. Quantities of interest (QOI) as a function of arrival date. QOI vs date of arrival that resulted in an epidemic by calendar date. The x-axis is the date of arrival of an infectious human, the simulation start date of February 15. The blue square points represent the time to peak infection in humans (in days). The red diamond points represent the maximum number of humans infected at any given point during the simulation. The green circle points represent the final (or cumulative) epidemic size at the end of the simulation; this is represented as the proportion of humans infected (rather than number). Simulations for arrivals dates in November/December, resulted in a prolonged low-level transmission, with bimodal peak, while other dates had a classical unimodal peak.

Overall, the shifts in epidemic dynamics are driven by the seasonal change (summer and autumn seasons) and its effect on transmission dynamics. Epidemic peak size was highest (with

20% of the susceptible population infected), for an arrival date on August 17 (at a starting temperature of 23.1°C), with a short time to peak of 65 days (Fig 2A) and. Epidemic peak size was lowest (with 5% of the susceptible population infected) for an arrival date on November 5 (at a starting temperature of 20.3°C), with a longer time to peak of 340 days (Fig 2C) and. All epidemic simulations ultimately infected 100% of the human population, except for arrival dates in late October to early November, with an average final epidemic size of 97% of the population (Fig 3).

These results show that under the conditions used here, an epidemic potential exists within the summer to early winter seasons, with most favorable seasons for a large outbreak being in mid-summer/early autumn season. Epidemics occurring within this favorable period had an average epidemic peak size of 18% of the susceptible population infected, with a time to peak of 70 days. Arrival dates of an infectious human, in late-autumn and early winter season, can dramatically affect the epidemic dynamics.

Seasonal variance and epidemic dynamics

To examine the epidemic dynamics as a function of the seasonal temperature variance, we simulated two different sets of temperature regimes, with a fixed arrival date in mid-summer (August 15). In the first set of temperature regimes (historical; T_{mean} varied from 19.0°C to 22.0°C and T_{range} varied from 4.0°C to 6.0°C, both in increments of 0.2°C), the timing and magnitude of the epidemic peak vary inversely as a function of starting temperature (calculated for August 15 from T_{mean} and T_{range} using equation 16). Epidemic peak size increases

monotonically with an increase in starting temperature, i.e. warmer temperatures at onset produce large epidemic peak size with a short peak time and vice versa (Fig 4A). The final epidemic size was insensitive to starting temperatures, as all simulations within this regime produced final epidemic sizes of 100% of the population infected.

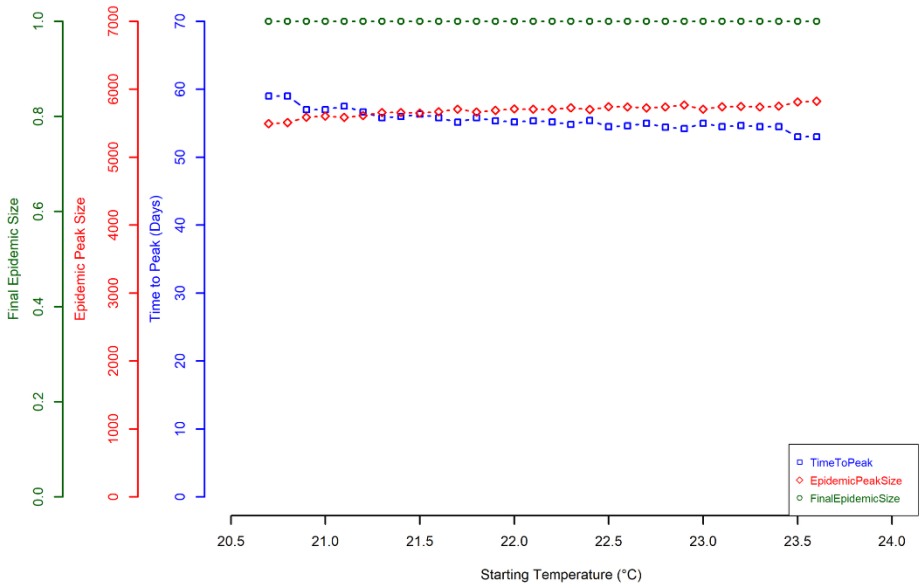

A

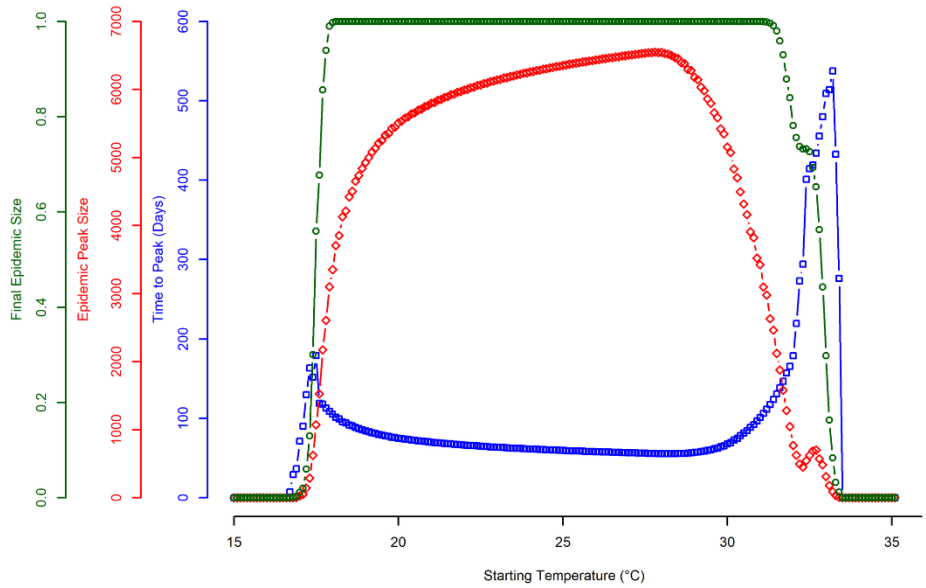

B

Fig 4. Quantities of interest (QOI) as a function of starting temperature. The x-axis is the starting temperatures within each set of temperature regimes and the y-axis is the associated value of the QOI being considered. Starting temperature is the temperature on August 15 calculated from T_{mean} and T_{range}. The blue square points represent the time to peak infection in humans (in days). The red diamond points represent the maximum number of humans infected at any given point during the simulation. The green circle points represent represents the final (or cumulative) epidemic size at the end of the simulation; this is represented as the proportion of humans infected (rather than number). (A) represents the historical temperature regimes, given by T_{mean} varied from 19°C to 22°C and T_{range} varied from 4°C to 6°C (both in increments of 0.2°C), a total of 121 simulations. (B) represents the second set of temperature regimes, given by T_{mean} varied from 15°C to 30°C and T_{range} varied from 0°C to 15.0°C, a total of 5776 simulations. Due to the fixed starting date, multiple combinations of T_{mean} and T_{range} had the same starting temperature. As no other parameters were varied in these simulation sets, QOI and model behavior was identical for simulations with the same starting temperatures and overlapping points are not visible on the graphs. The default parameters from Table 2 were used for these simulations.

In the second set of temperature regimes (future; T_{mean} varied from 15.0°C to 30.0°C and T_{range} varied from 0.0°C to 15.0°C, both in increments of 0.2°C), epidemic peak time and size show similar inverse variation as a function of starting temperature, although the overall behavior is different. Epidemic peak size had a unimodal distribution with its peak at ~28 ºC and steadily declines afterward (conversely the time to peak decreases until ~30 ºC). At this peak of ~28 ºC, the epidemic peak size was at 22% of the susceptible population infected, within a short peak time of 55 days. On the other hand, the final epidemic size steeply increases as a function of starting temperature, and plateaus at 18 ºC to 32 ºC (with 100% of the population infected), before steeply declining (Fig 4B). Extending the temperature regimes demonstrates the nonlinear influence of the interaction between mean temperature and seasonal variance on the epidemic dynamics.

To further examine this, Fig 5 shows the variation in the final epidemic size across the annual temperature bands. At a low mean annual temperature of 15ºC to 17ºC and range of 0ºC to ~7.5ºC, no epidemic occurred; however, this temperature band becomes suitable for transmission as the temperature range increases beyond this point. Mean annual temperature of ~18ºC to ~28ºC, supports epidemic transmission at both low and high-temperature ranges. Epidemics introduced within these temperature regimes had the highest epidemic suitability (using final epidemic size as a measure of epidemic suitability). Lastly, mean annual temperature bands of ~28ºC to 30ºC and low range of 0ºC to ~7.5ºC, transmission was supported with high epidemic suitability, this steadily diminishes as temperature range increases. In general, under the conditions used here, the dynamics of the epidemic are largely driven by the seasonal variation in temperature.

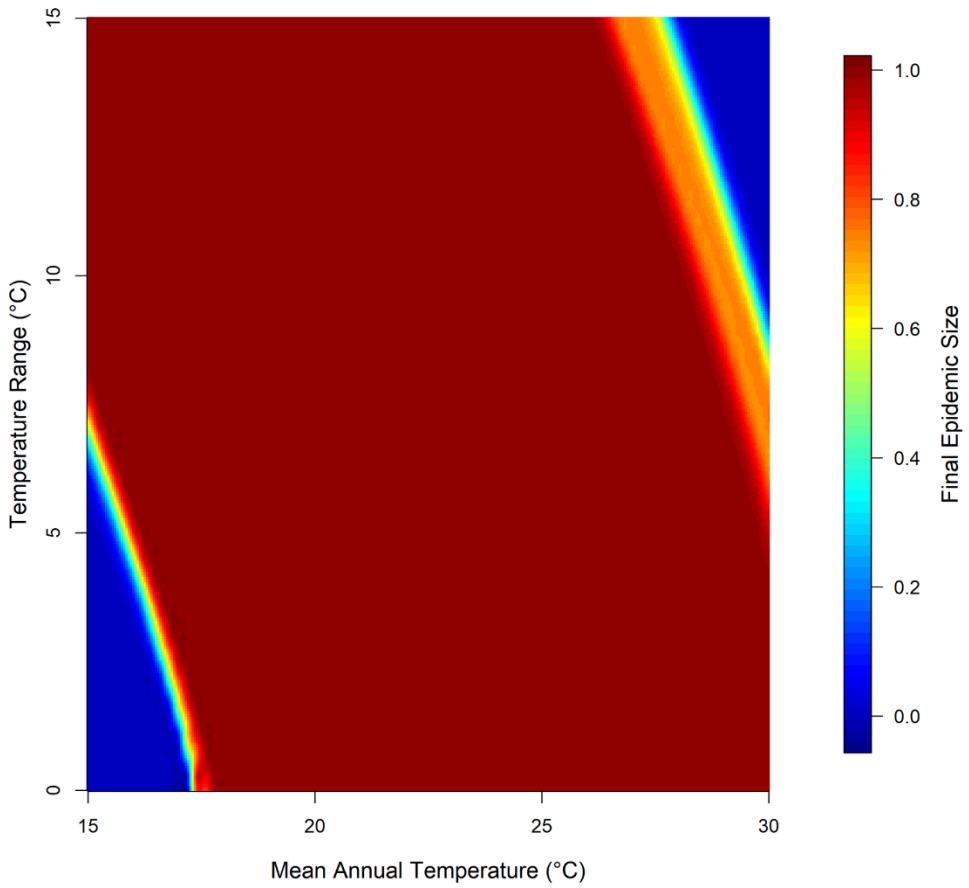

Fig 5. Final epidemic size across different seasonal temperature regimes. Heat map of final epidemic size (represented as the proportion of humans infected rather than number) as a function of mean annual temperature and temperature range. Temperature regimes here is given by T_{mean} varied from 15°C to 30°C and T_{range} varied from 0°C to 15°C, a total of 5776 simulations. Default parameters from Table 2 were used for these simulations, except for temperature parameters.

Model sensitivity analysis

Model sensitivity was characterized using 500 simulations runs for dengue parameter ranges as given in Table 2. All parameters were uniformly distributed for the LHS sampling. The conditions here were permissive for epidemics, with ($I_h > 2$) in 392 of the 500 simulated parameters set. The epidemic progression in these parameter sets was consistent with the general model behavior seen in Figs 2A and 2C (i.e. a combination of unimodal and bimodal responses). The distribution of the QOI had a wider range of values (i.e. $MaxI_h$ = 3 to 8514 humans infected; $tmaxI_h$ = 16 to 365 days from t_{crit}; $cumI_h$ = 0.01% to 100% of the population infected), thus providing adequate variation for the sensitivity analysis.

Table 3 shows the relative importance of the input parameters to our QOI, using uniform LHS distributions for dengue parameters (Table 2). Considering the main effects only, our QOI were all sensitive to the arrival date of the infectious human and mean annual temperature, and less sensitive to temperature range. Other influential parameters on all the QOI were the mosquito biting rate, transmission rates, and mosquito recruitment. The time to epidemic peak was less sensitive to the mosquito life-history trait parameters in comparison to other QOI (Table 3).

Table 3. Sensitivity analysis of the model's quantities of interest (QOI).

Parameter	$MaxI_h$	$tmaxI_h$	$cumI_h$
t_{crit}	1.00 (0.17)	1.00 (0.21)	1.00 (0.30)
T_{mean}	0.99 (0.40)	1.00 (0.20)	1.00 (0.27)
T_{range}	0.41 (0.40)	0.47 (-0.03)	0.67 (-0.05)
a	1.00 (-0.20)	1.00 (0.12)	0.99 (-0.13)
$\beta_{h\to v}$	1.00 (0.33)	0.71 (0.06)	1.00 (0.27)
$\beta_{v\to h}$	0.99 (0.18)	1.00 (-0.15)	0.73 (0.06)
μ_v	1.00 (-0.41)	0.24 (0.00)	1.00 (-0.19)
γ_v	0.42 (0.07)	0.43 (-0.02)	0.29 (0.00)
iv	0.28 (0.01)	0.26 (0.00)	0.27 (0.00)
q	0.34 (0.21)	0.32 (0.01)	0.40 (0.02)
R_{tot}	1.00 (0.28)	0.32 (0.01)	0.98 (0.12)

Relative importance and model-averaged parameter coefficient from best-supported models (confidence set of models, see S2 appendix for details). The relative importance of parameters on a scale between 0.00 and 1.00; the model-averaged coefficients for parameters in parentheses - effects are summarized by their direction $(+|-)$, positive indicates the QOI increases as the parameter increases, while negative indicates QOI decreases as the parameter increases. Before model fitting, parameters were centered on zero and scaled to unit variance, to normalize parameters within the same range, hence coefficient estimates are within the range of 0.0 to 1.0. QOI is denoted by: $maxI_h$ = the epidemic peak size; $tmaxI_h$ = time to peak; $cumI_{\mathrm{h}}$ = final epidemic size. Notations and descriptions of parameters are denoted in Table 2.

All the QIO were sensitive to the interaction term between the arrival date of an infectious human and temperature range, and less sensitive to the interaction term of arrival date and mean annual temperature. Some other interactive terms that were influential to all QOI include interactions (terms) between arrival date of an infectious human and the mosquito life-

history trait parameters (i.e. biting rate, transmission rates, and recruitment). Interactions between transmission rates and other parameters had high relative importance for epidemic peak and final sizes, indicating that transmission rates may alter the effect of other parameters (See S8 Table for full details).

Discussion

We extend the Lord et al. (unpublished work) model for chikungunya in *Aedes aegypti* and *Aedes albopictus* mosquitoes in Florida to a deterministic compartmental model for dengue fever in *Aedes aegypti* in Madeira Island. This SEI-SEIR model explores dengue epidemic dynamics as triggered by the arrival of an infected person in Funchal, Madeira and the effects of seasonally varying temperature on transmission. Our analysis focused on three quantities of interest: time to epidemic peak, epidemic peak size and the final size of the epidemic. We then used a global sensitivity analysis to determine which input parameters were most important to quantities of interest.

Our model demonstrates that the date of arrival of an infected human in the susceptible human population dramatically affects the overall epidemic dynamics. With arrivals in mid-summer (July) to early-autumn (September) producing epidemics at a faster peak rate and a resulting large final epidemic size. These transient epidemics are indicative of a higher transmission potential at this point of the year and are consistent with the scenario of the 2012 outbreak [6]. Our results are also consistent with the conclusions of [8], regarding the time point in the year with the highest epidemic risk and when local control strategies should be intensified.

The overall model behavior in response to the timing of virus introduction within the susceptible population is similar to other previous dengue models [26, 57].

Furthermore, our results show the interaction between seasonal temperature mean and variance on the epidemic dynamics. The temperature seasonality for Funchal, Madeira, demonstrated a highly suitable thermal environment for the vectorial capacity of *Aedes aegypti* mosquitoes and arbovirus transmission. As expected, all our model simulations for these temperature regimes evolved into an epidemic, with warmer temperatures at onset producing high prevalence and faster peaks. Our subsequent extension of the temperature regimes demonstrates the nonlinear influence of temperature seasonality on the epidemic dynamics. Likewise, it allowed us to examine plausible future forcing scenarios based on near-term projections of seasonal temperature changes. Overall, the thermal responses from both temperature regimes were similar to those discussed in the works of [17] and [18], which investigated the effects of temperature on dengue transmission.

Our sensitivity analysis further characterizes the variability of the epidemic dynamics to other parameters in our model. Beyond the arrival date of an infected human and temperature seasonality, the quantities of interest were also sensitive to the biting rate, transmission rates, and mosquito population size. This is consistent with other modeling studies that highlight the importance of the mosquito dynamics on epidemic outcomes [27, 58, 59]. Our sensitivity analysis went a step further to characterize the interaction effects of our model parameters. An example is the interaction term between mean temperature and other mosquito life-history traits (e.g. biting rates and population size), as demonstrated in other previous models (e.g. [13, 19,

60]). Though this was not the focus of our analysis, it can be useful in improving understanding of the complex processes that interact to determine epidemic dynamics. Likewise, from a control and mitigation perspective, the interaction term effects are useful to understand how the implementation of a specific control strategy can have dramatic effects on the mosquito life-history traits and in turn the overall epidemic dynamics. A cautionary note, our sensitivity analysis varied only the mosquito portion of the transmission cycle and does not account for the variance in the human transmission and its combined influence on the epidemic dynamics.

Putting this all together, our model is a useful mathematical tool to study different epidemic scenarios and shifts in epidemic suitability for other regions on the island, other than the south coast region, where Funchal is located. The model temperature seasonality was parameterized using the observed temperature of Funchal; however, the results can be extrapolated to other regions on the island. The near term projection for seasonal temperature variation for the region of Madeira island (i.e. the North Atlantic, Europe, and Mediterranean region), predicts a warming of ~2°C in annual mean temperature, with summer months of June, July and August (JJA) temperatures warming up to ~2.9°C [46, 51]. Given our results, we can speculate that the north coast and inland regions of the island, where current annual mean temperatures (e.g. Santana, a municipality in the north region with annual temperatures of 16.7ºC) suggests limited or no epidemic suitability could have an increased potential to support transmission in the near future. While the south coast region would continue to support transmission, with possible higher epidemic suitability. To reiterate, most of the simulated temperatures are very unlikely to occur on the island, except for sporadic extreme summer temperatures and heatwaves. Such sporadic extreme events have been documented, with recent

abrupt changes in temperatures on the island [52, 53]. Hence our simulations give an estimate of epidemic suitability in the likelihood of these extreme temperature conditions. Also, our results can apply to other islands, within the Macaronesia ecoregion with similar climatic conditions like Madeira. For example, the island of Santiago, located in the archipelago of Cape Verde, with similar *Aedes aegypti* population. Our results can provide insights into epidemic suitability shifts and a potential outbreak of dengue on this island. It is important to note that in real life, these projected shifts in epidemic suitability, will also be influenced by other factors like rainfall, humidity, and anthropogenic activities. Thus, seasonal temperature variation must be considered jointly with these factors.

Our model did not explicitly address the scenario of multiple serotypes of dengue co-circulating in the population, and the possibility of prior exposure leading to immune interactions and increased risk of severe disease (a possibility for Funchal, given the circulating serotype for the 2012 outbreak was DENV I). However, we made the following assumption when setting the constants for the human components of the transmission cycle. We consider that infection by a serotype produces permanent immunity to it, and temporal immunity to other serotypes [42, 61, 62]. Thus, we assumed that individuals infected from the 2012 outbreak, while they have permanent immunity to the DENV-1 serotype they remain susceptible to other serotypes. Hence the constants for the intrinsic incubation and infectious periods were set to reflect an introduction of a different serotype other than DENV-1. These constants reflect mean values for DENV-2 and DENV-4 as reported in previous literature [36, 40-43]. The analysis presented here is relevant for the introduction of a new serotype on the island, which is timely in the light of the work of [22]. Their study had demonstrated the ability of the *Aedes aegypti* populations from Madeira to

transmit DENV-2, and the potential risk for the local transmission if introduced to Madeira. Our results suggest that the epidemic dynamics would be significantly impacted by the introduction of a different serotype in comparison to the 2012 outbreak. This emphasizes the crucial need for the island to intensify its control measures to prevent local transmission while preparing effective mitigation strategies in the event of another outbreak.

In summary, the model presented here is relevant for the introduction of a new dengue serotype into Funchal, Madeira Island and the interaction between mean temperature and seasonal variation to drive the epidemic dynamics. Our results demonstrate the potential for summer to early winter transmission of dengue, with varying levels of epidemic suitability, following an introduction of the virus. Overall, we demonstrated that epidemic dynamics are strongly influenced by variation in the date of arrival, seasonal temperature, biting rate, transmission rates, and the mosquito population. The model sensitivity analysis provides insight into the relative importance of these parameters and their interactive effects as mechanistic drivers of an epidemic. These results can be a useful guide in the development of effective local control and mitigation strategies for dengue fever in Madeira Island.

Acknowledgments

We appreciate Joe Pohedra who assisted in the programming of the initial transmission model and Jebidiah Light who assisted with the adaption to the current SEI-SEIR model.

References

1. Messina JP, Brady OJ, Golding N, Kraemer MUG, Wint GRW, Ray SE, et al. The current and future global distribution and population at risk of dengue. Nat Microbiol. 2019. doi: https://doi.org/10.1038/s41564-019-0476-8.

2. Kraemer MUG, Hay SI, Pigott DM, Smith DL, Wint GRW, Golding N. Progress and challenges in infectious disease cartography. Trends Parasitol. 2016;32(1):19-29. doi: https://doi.org/10.1016/j.pt.2015.09.006.

3. Leta S, Beyene TJ, De Clercq EM, Amenu K, Kraemer MUG, Revie CW. Global risk mapping for major diseases transmitted by *Aedes aegypti and Aedes albopictus*. Int J Infect Dis. 2018;67:25-35. doi: https://doi.org/10.1016/j.ijid.2017.11.026.

4. Margarita Y, Grácio AS, Lencastre I, Silva A, Novo T, Sousa C. First record of *Aedes (stegomyia) aegypti* (Linnaeus, 1762) (Diptera, culicidae) in Madeira Island - Portugal (in portguese) Acta Parasitol Port.. 2006;13:59-61.

5. Medlock JM, Hansford KM, Schaffner F, Versteirt V, Hendrickx G, Zeller H, et al. A review of the invasive mosquitoes in Europe: ecology, public health risks, and control options. Vector Borne Zoonotic Dis. 2012;12(6):435-47. doi: https://doi.org/10.1089/vbz.2011.0814.

6. ECDC. Dengue outbreak in madeira (2012-13) 2013. European Centre for Disease Prevention and Control [17 Jul 2019]. Available from: https://ecdc.europa.eu/en/dengue-fever/threats-and-outbreaks/madeira-outbreak-2012.

7. ECDC. Update on autochthonous dengue cases in Madeira, Portugal. Stockholm: European Centre for Disease Prevention and Control, 2012. Available from: https://ecdc.europa.eu/sites/portal/files/media/en/publications/Publications/dengue-madeira-risk-assessment-update.pdf.

8. Lourenco J, Recker M. The 2012 Madeira dengue outbreak: epidemiological determinants and future epidemic potential. PLoS Negl Trop Dis. 2014;8(8):e3083. doi: https://doi.org/10.1371/journal.pntd.0003083.

9. Watts DM, Burke DS, Harrison BA, Whitmire RE, Nisalak A. Effect of temperature on the vector efficiency of *Aedes aegypti* for dengue 2 virus. Am J Trop Med Hyg.1987;36(1):143-52. doi: https://doi.org/10.4269/ajtmh.1987.36.143.

10. Rueda LM, Patel KJ, Axtell RC, Stinner RE. Temperature-dependent development and survival rates of *Culex quinquefasciatus* and *Aedes aegypti* (Diptera: Culicidae). J Med Entomol. 1990;27(5):892-8. doi: https://doi.org/10.1093/jmedent/27.5.892

11. Eisen L, Monaghan AJ, Lozano-Fuentes S, Steinhoff DF, Hayden MH, Bieringer PE. The impact of temperature on the bionomics of *Aedes (stegomyia) aegypti*, with special reference to the cool geographic range margins. J Med Entomol. 2014;51(3):496-516. doi: https://doi.org/10.1603/ME13214.

12. Couret J, Dotson E, Benedict MQ. Temperature, larval diet, and density effects on development rate and survival of *Aedes aegypti* (Diptera: Culicidae). PloS One. 2014;9(2):e87468. doi: https://doi.org/10.1371/journal.pone.0087468.

13. Yang HM, Macoris ML, Galvani KC, Andrighetti MT, Wanderley DM. Assessing the effects of temperature on the population of *Aedes aegypti*, the vector of dengue. Epidemiol Infect. 2009;137(8):1188-202. doi: https://doi.org/10.1017/s0950268809002040.

14. Johansson MA, Powers AM, Pesik N, Cohen NJ, Staples JE. Nowcasting the spread of chikungunya virus in the Americas. PloS One. 2014;9(8):e104915. doi: https://doi.org/10.1371/journal.pone.0104915.

15. Liu-Helmersson J, Stenlund H, Wilder-Smith A, Rocklöv J. Vectorial capacity of *Aedes aegypti*: effects of temperature and implications for global dengue epidemic potential. PloS One. 2014;9(3):e89783. doi: https://doi.org/10.1371/journal.pone.0089783.

16. Morin CW, Monaghan AJ, Hayden MH, Barrera R, Ernst K. Meteorologically driven simulations of dengue epidemics in San Juan, PR. PLoS Negl Trop Dis. 2015;9(8):e0004002. doi: https://doi.org/10.1371/journal.pntd.0004002.

17. Mordecai EA, Cohen JM, Evans MV, Gudapati P, Johnson LR, Lippi CA, et al. Detecting the impact of temperature on transmission of zika, dengue, and chikungunya using mechanistic models. PLoS Negl Trop Dis. 2017;11(4):e0005568. doi: https://doi.org/10.1371/journal.pntd.0005568.

18. Huber JH, Childs ML, Caldwell JM, Mordecai EA. Seasonal temperature variation influences climate suitability for dengue, chikungunya, and zika transmission. PLoS Negl Trop Dis. 2018;12(5):e0006451. doi: https://doi.org/10.1371/journal.pntd.0006451.

19. Mordecai EA, Caldwell JM, Grossman MK, Lippi CA, Johnson LR, Neira M, et al. Thermal biology of mosquito-borne disease. Ecol Lett. 2019;0(0). doi: https://doi.org/10.1111/ele.13335.

20. Fernandopullé D. Climatic characteristics of the Canary Islands. In: G. K, editor. Biogeography and ecology in the Canary Islands: Springer, Dordrecht; 1976. p. 185-206.

21. Santos FD, Valente MA, Miranda PMA, Aguiar A, Azevedo EB, Tomé AR, et al. Climate change scenarios in the Azores and Madeira Islands. World Resour Rev. 2004;16(4):473-91. http://idlcc.fc.ul.pt/pdf/SantosEtalWRR2004.pdf.

22. Seixas G, Jupille H, Yen P-S, Viveiros B, Failloux A-B, Sousa CA. Potential of *Aedes aegypti* populations in Madeira Island to transmit dengue and chikungunya viruses. Parasit Vectors. 2018;11(1):509. doi: https://doi.org/10.1186/s13071-018-3081-4.

23. Messina JP, Brady OJ, Pigott DM, Brownstein JS, Hoen AG, Hay SI. A global compendium of human dengue virus occurrence. Sci Data. 2014;1:140004. doi: https://doi.org/10.1038/sdata.2014.4.

24. Guo C, Zhou Z, Wen Z, Liu Y, Zeng C, Xiao D, et al. Global epidemiology of dengue outbreaks in 1990-2015: A systematic review and meta-analysis. Front Cell Infect Microbiol. 2017;7:317-. doi: https://doi.org/10.3389/fcimb.2017.00317.

25. Ryan SJ, Carlson CJ, Mordecai EA, Johnson LR. Global expansion and redistribution of Aedes-borne virus transmission risk with climate change. PLoS Negl Trop Dis. 2019;13(3):e0007213. doi: https://doi.org/10.1371/journal.pntd.0007213.

26. Otero M, Solari HG. Stochastic eco-epidemiological model of dengue disease transmission by *Aedes aegypti* mosquito. Math Biosci. 2010;223(1):32-46. doi: https://doi.org/10.1016/j.mbs.2009.10.005.

27. Manore CA, Hickmann KS, Xu S, Wearing HJ, Hyman JM. Comparing dengue and chikungunya emergence and endemic transmission in *A. aegypti* and *A. albopictus*. J Theor Biol. 2014;356:174-91. doi: https://doi.org/10.1016/j.jtbi.2014.04.033.

28. Karl S, Halder N, Kelso JK, Ritchie SA, Milne GJ. A spatial simulation model for dengue virus infection in urban areas. BMC Infect Dis. 2014;14:447. doi: https://doi.org/10.1186/1471-2334-14-447.

29. Ferreira CP, Godoy WAC. Ecological modelling applied to entomology. Switzerland: Springer; 2014.

30. Institute of Health Administration, IP-RAM. Mosquito on Madeira Island (in Portuguese). Institute of Health Administration, IP-RAM, Regional Secretariat of Health, Autonomous Region of Madeira; 2019 [17 Jul 2019]. Available from: http://doc.iasaude.pt/mosquito/index.php/mosquito/mosquito-na-ilha-da-madeira.

31. Duong V, Lambrechts L, Paul RE, Ly S, Lay RS, Long KC, et al. Asymptomatic humans transmit dengue virus to mosquitoes. Proc Natl Acad Sci . 2015;112(47):14688-93. doi: https://doi.org/10.1073/pnas.1508114112.

32. Newton EA, Reiter P. A model of the transmission of dengue fever with an evaluation of the impact of ultra-low volume (ulv) insecticide applications on dengue epidemics. The Am J Trop Med Hyg. 1992;47(6):709-20. doi: https://doi.org/10.4269/ajtmh.1992.47.709.

33. Menach AL, McKenzie FE, Flahault A, Smith DL. The unexpected importance of mosquito oviposition behaviour for malaria: non-productive larval habitats can be sources for malaria transmission. Malar J. 2005;4(1):23. doi: https://doi.org/10.1186/1475-2875-4-23.

34. Institute of Health Administration, IP-RAM. Entomological panel bulletins(in Portuguese). IASAÚDE IP-RAM, Sanitary Engineering Unit: Institute of Health Administration, IP-RAM, Regional Secretariat of Health, Autonomous Region of Madeira, 2019. Available from: http://doc.iasaude.pt/mosquito/index.php/boletins/entomologicos.

35. Trpis M, Hausermann W. Dispersal and other population parameters of Aedes aegypti in an African village and their possible significance in epidemiology of vector-borne diseases. Am J Trop Med Hyg. 1986;35(6):1263 - 79. doi: https://doi.org/10.4269/ajtmh.1986.35.1263.

36. Lourenco J, Recker M. Dengue serotype immune-interactions and their consequences for vaccine impact predictions. Epidemics. 2016;16:40-8. doi: https://doi.org/10.1016/j.epidem.2016.05.003.

37. Paupy C, Ollomo B Fau - Kamgang B, Kamgang B Fau - Moutailler S, Moutailler S Fau - Rousset D, Rousset D Fau - Demanou M, Demanou M Fau - Herve J-P, et al. Comparative role of Aedes albopictus and Aedes aegypti in the emergence of dengue and chikungunya in central Africa. Vector Borne Zoonotic Dis. 2010;10(3). doi: https://doi.org/10.1089/vbz.2009.0005.

38. Lord CC. The effect of multiple vectors on arbovirus transmission. Isr J Ecol Evol. 2010;56(3-4):371-92. doi: https://doi.org/10.1560/ijee.55.3-4.371.

39. Focks DA, Barrera R. Dengue transmission dynamics: Assessment and implications for control. CiteSeer: World health organization on behalf of the special programme for research and training in tropical diseases, 2007. Available from: http://citeseerx.ist.psu.edu/viewdoc/summary?doi=10.1.1.612.689.

40. Nishiura H, Halstead SB. Natural history of dengue virus (DENV)-1 and DENV-4 infections: reanalysis of classic studies. J Infect Dis. 2007;195(7):1007–13. doi: https://doi.org/10.1086/511825.

41. Chan M, Johansson MA. The incubation periods of dengue viruses. PloS One. 2012;7(11):e50972. doi: https://doi.org/10.1371/journal.pone.0050972.

42. Gubler DJ, Suharyono W, Tan R, Abidin M, Sie A. Viraemia in patients with naturally acquired dengue infection. Bull World Health Organ. 1981;59(4):623-30. https://www.ncbi.nlm.nih.gov/pubmed/6976230.

43. Vaughn DW, Green S, Kalayanarooj S, Innis BL, Nimmannitya S, Suntayakorn S, et al. Dengue viremia titer, antibody response pattern, and virus serotype correlate with disease severity. J Infect Dis. 2000;181(1):2-9. doi: https://doi.org/10.1086/315215.

44. Santo António Parish Council. History of Santo António parish council (in Portuguese): junta de freguesia de Santo António- an autonomous region of Madeira; 2018 [17 Jul 2019]. Available from: http://www.jf-santoantonio.pt/historia.

45. Weather Underground. Weather history for Funchal Madeira (2008-2018) 2019 [01 Mar 2019]. Available from: https://www.wunderground.com/history/daily/pt/funchal/LPMA.

46. IPCC. Climate change 2013: The physical science basis. Contribution of working group i to the fifth assessment report of the intergovernmental panel on climate change. Cambridge University Press, Cambridge, United Kingdom, and New York, NY, USA: 2013; [1535]. Available from: https://www.ipcc.ch/report/ar5/wg1/.

47. Funchal city hall. Funchal natural history museum: Funchal city hall (Câmara Municipal do Funchal) 2019. Available from: http://www.cm-funchal.pt/pt/servi%C3%A7os/ci%C3%AAncia/museu-de-hist%C3%B3ria-natural-do-funchal/sobre-o-museu.html.

48. Andraud M, Hens N, Marais C, Beutels P. Dynamic epidemiological models for dengue transmission: a systematic review of structural approaches. PloS One. 2012;7(11):e49085. doi: https://doi.org/10.1371/journal.pone.0049085.

49. Kiraly A, Janosi IM. Stochastic modeling of daily temperature fluctuations. Phys Rev. 2002;65(1539-3755 (Print)):051102 1-6. doi: https://doi.org/10.1103/PhysRevE.65.051102.

50. Lord CC, Day JF. Simulation studies of st. Louis encephalitis virus in south Florida. Vector Borne Zoonotic Dis. 2001;1(4):299-315. doi: https://doi.org/10.1089/15303660160025921.

51. Seneviratne SI, Field CB, Barros V, Stocker TF, Dahe Q, Dokken DJ, et al. Managing the risks of extreme events and disasters to advance climate change adaptation. Cambridge: Intergovernmental panel on climate change 2012; [582]. Available from: https://www.ipcc.ch/report/managing-the-risks-of-extreme-events-and-disasters-to-advance-climate-change-adaptation/.

52. Madeira Island News. Madeira heatwave continues. Madeira Island News, 2016 [17 Jul 2019]. Available from: https://www.madeiraislandnews.com/2016/08/heatwave-continues.html.

53. Madeira Island News. Hottest December day for 150 years. Madeira Island News, 2018 [17 Jul 2019]. Available from: https://www.madeiraislandnews.com/2018/12/hottest-december-day-for-150-years.html.

54. MathWorks. MATLAB and Statistics Toolbox Release 2016a. Natick, Massachusetts: The MathWorks Inc.; 2016.

55. Calcagno V, de Mazancourt C. Glmulti: an R package for easy automated model selection with (generalized) linear models. 2010. 2010;34(12): J Stat Softw. doi: https://doi.org/10.18637/jss.v034.i12.

56. R-Core-Team. The R project for statistical computing: CRAN; 2019. Available from: https://www.r-project.org/.

57. Erickson RA, Presley SM, Allen LJS, Long KR, Cox SB. A dengue model with a dynamic Aedes albopictus vector population. Ecol Model. 2010;221(24):2899-908. doi: https://doi.org/10.1016/j.ecolmodel.2010.08.036.

58. Ellis AM, Garcia AJ, Focks DA, Morrison AC, Scott TW. Parameterization and sensitivity analysis of a complex simulation model for mosquito population dynamics, dengue

transmission, and their control. Am J Trop Med Hyg. 2011;85(2):257-64. doi: https://doi.org/10.4269/ajtmh.2011.10-0516.

59. Ndii MZ, Hickson RI, Allingham D, Mercer GN. Modelling the transmission dynamics of dengue in the presence of Wolbachia. Math Biosci. 2015;262:157-66. doi: https://doi.org/10.1016/j.mbs.2014.12.011.

60. Yang HM, Macoris ML, Galvani KC, Andrighetti MT, Wanderley DM. Assessing the effects of temperature on dengue transmission. Epidemiol Infect. 2009;137(8):1179-87. doi: https://doi.org/10.1017/s0950268809002052.

61. Wearing HJ, Rohani P. Ecological and immunological determinants of dengue epidemics. Proc Natl Acad Sci . 2006;103(31):11802-7. doi: https://doi.org/10.1073/pnas.0602960103.

62. Esteva L, Vargas C. Coexistence of different serotypes of dengue virus. J Math Biol. 2003;46(1):31-47. doi: https://doi.org/10.1007/s00285-002-0168-4.

Supporting information

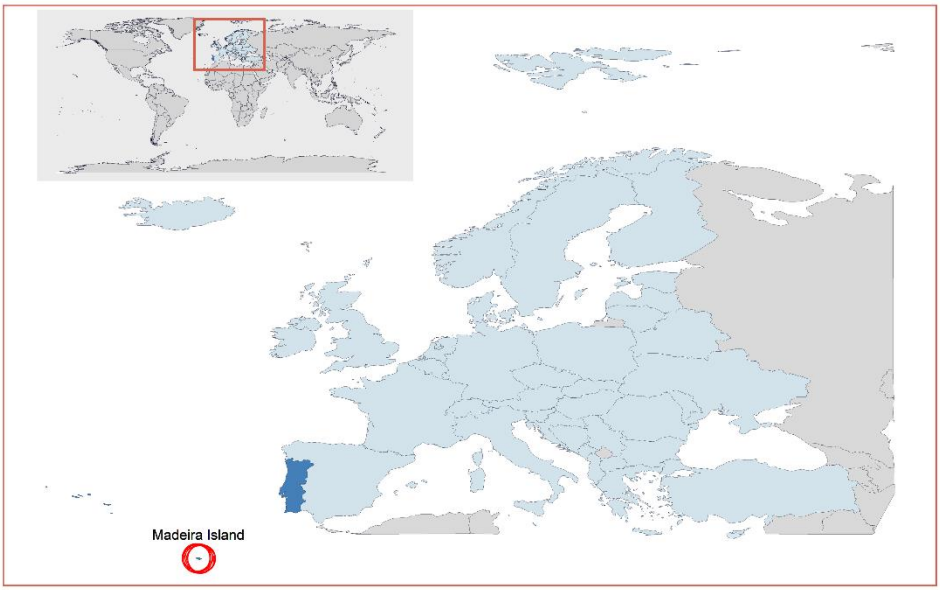

S1 Fig. Location of Madeira Island. Map of Europe in light blue, Portugal and Azorean islands in dark blue, Madeira island circled in red.

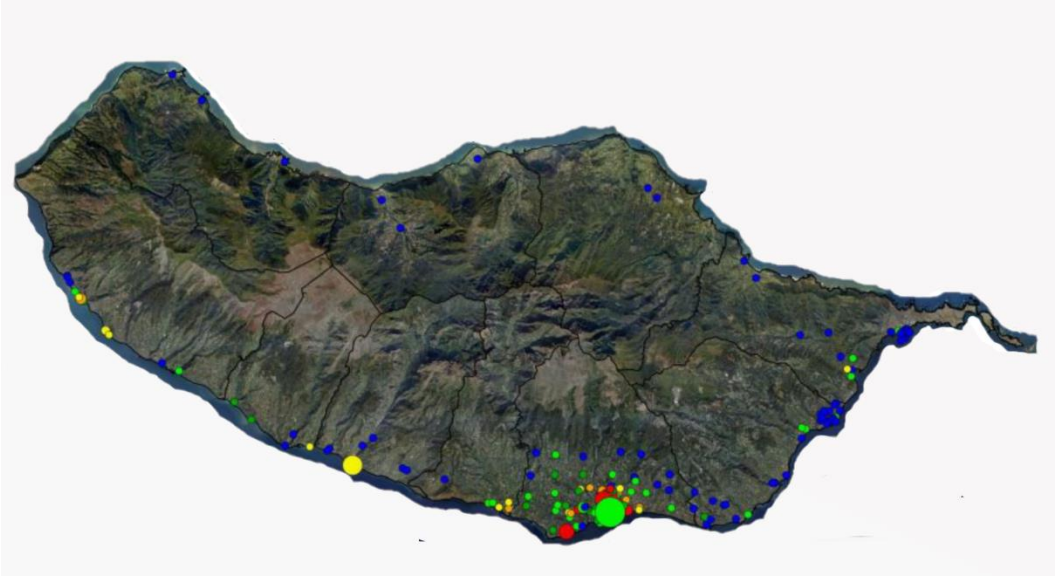

S2 Fig. Location of Ovitraps in Madeira Island. The distribution of ovitrap location across the island, as reported in the Entomological panel bulletins (PEnt_RAMW52/2019, in Portuguese) of the Institute of Health Administration, IP-RAM (IASAÚDE IP-RAM). The colored dots on the map, represents the cumulative number of eggs in each location for the week 10, 2018 to week 52, 2019. Blue = 0%, Dark green =1%-10%, Light green =11% - 20%, Yellow=21% -30%, Orange= 31% -40%, Red=41% -100%. Cumulative number of eggs for all location= 37766. Adapted from Institute of Health Administration, IP-RAM [34]

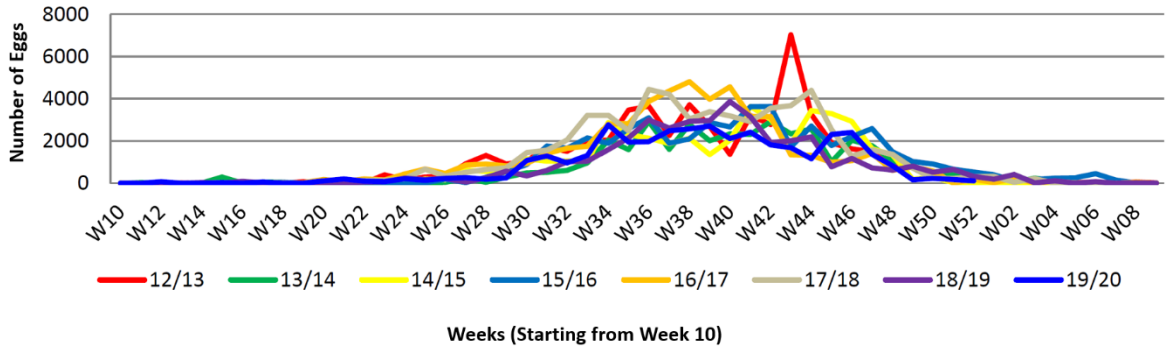

S3 Fig. Cumulative results of Ovitraps in Madeira Island. Annual cumulative number of eggs reported across the island from all the ovitraps, as reported in the Entomological panel bulletins (PEnt_RAMW52/2019, in Portuguese) of the Institute of Health Administration, IP-RAM (IASAÚDE IP-RAM). Entomological year starts from week 10. Graphs shows cumulative number of eggs for week 10, 2012 to week 52, 2019, with each entomological year represented in a different line color. Adapted from Institute of Health Administration, IP-RAM [34]

S4 Fig. Location of BG-traps in Madeira Island. The distribution of BG-traps location across the island, as reported in the Entomological panel bulletins (PEnt_RAMW52/2019, in Portuguese) of the Institute of Health Administration, IP-RAM (IASAÚDE IP-RAM). The colored dots on the map, represents the cumulative number of adult mosquitoes in each location for the week 10, 2018 to week 52, 2019. Blue = 0%, Dark green =1%-10%, Light green =11% -30%, Yellow=31% -50%, Orange= 51% -60%, Red=61% -100%. Cumulative number of adult mosquitoes for all location= 3464. Adapted from Institute of Health Administration, IP-RAM [34]

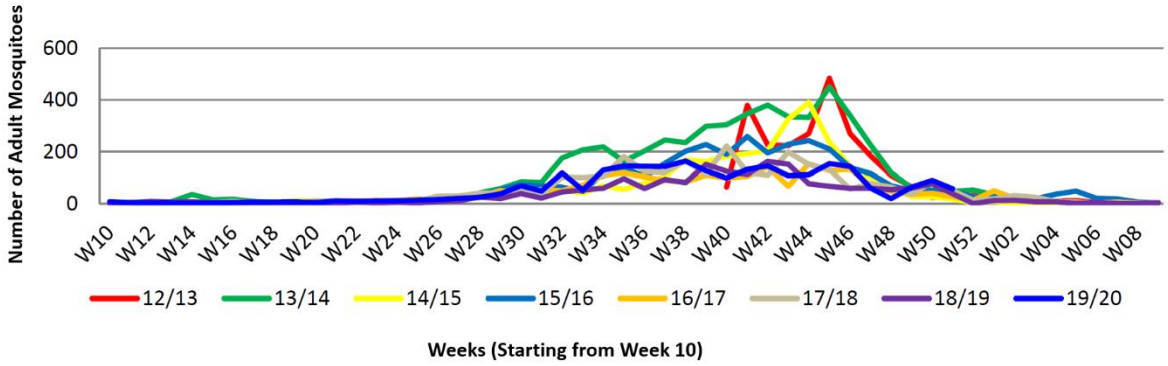

S5 Fig. Cumulative results of BG-traps in Madeira Island. Annual cumulative number of adult mosquitos reported across the island from all the BG-traps, as reported in the Entomological panel bulletins (PEnt_RAMW52/2019, in Portuguese) of the Institute of Health Administration, IP-RAM (IASAÚDE IP-RAM). Entomological year starts from week 10.

Graphs shows cumulative number of eggs for week 40, 2012 to week 52, 2019, with each entomological year represented in a different line color. Adapted from Institute of Health Administration, IP-RAM [34]

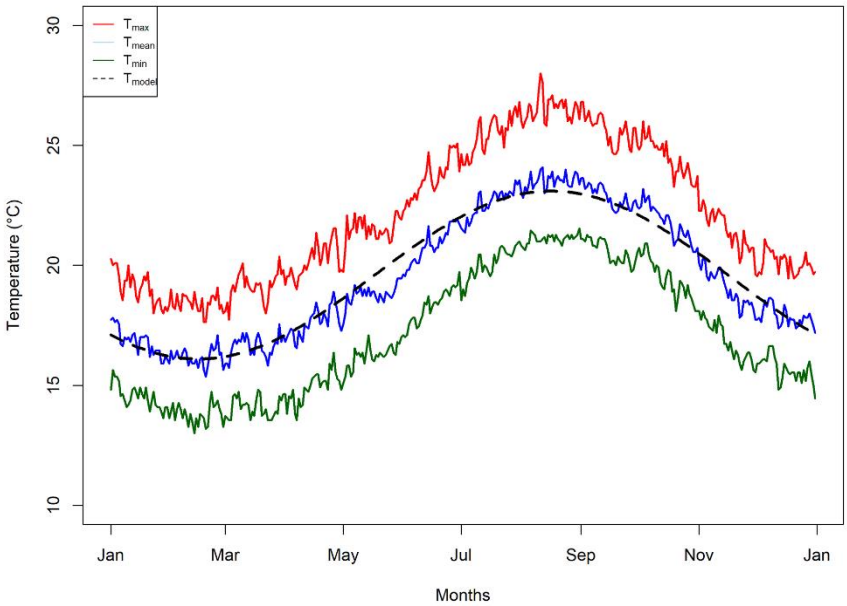

S6 Fig. Seasonal temperature pattern. The temperature seasonality pattern as observed from the historical decadal data for Funchal, Madeira. Average of minimum (green line), mean (blue line) and maximum (red line) temperatures per day between 2008 and 2018. Black dashed line is daily mean temperature of our model as calculated from sinusoidal curve (Equation 16 in the main article). The long-term average conditions in Funchal, Madeira T_{max}= 22°C, T_{mean}= 20°C, T_{min}= 17°C. Average mean temperatures for the spring months (Mar – May) was 18°C; Summer months (Jun – Aug) was 22°C; Autumn months (Sep – Nov) was 21°C and Winter months (Dec – Feb) was 17°C.

S1 File. S1 Appendix. Model starting conditions

S2 File. S2 Appendix. Model sensitivity analysis and multi-model inference analysis